Representing Grass– and Shrub–Snow–Atmosphere Interactions in Climate System Models

GLEN E. LISTON

Cooperative Institute for Research in the Atmosphere, Colorado State University, Fort Collins, Colorado

CHRISTOPHER A. HIEMSTRA

U.S. Army Cold Regions Research and Engineering Laboratory, Fort Wainwright, Alaska

(Manuscript received 25 August 2010, in final form 18 November 2010)

ABSTRACT

A vegetation-protruding-above-snow parameterization for earth system models was developed to improve energy budget calculations of interactions among vegetation, snow, and the atmosphere in nonforested areas. These areas include shrublands, grasslands, and croplands, which represent 68% of the seasonally snow-covered Northern Hemisphere land surface (excluding Greenland). Snow depth observations throughout nonforested areas suggest that mid- to late-winter snowpack depths are often comparable or lower than the vegetation heights. As a consequence, vegetation protruding above the snow cover has an important impact on snow-season surface energy budgets. The protruding vegetation parameterization uses disparate energy balances for snow-covered and protruding vegetation fractions of each model grid cell, and fractionally weights these fluxes to define grid-average quantities. SnowModel, a spatially distributed snow-evolution modeling system, was used to test and assess the parameterization. Simulations were conducted during the winters of 2005/06 and 2006/07 for conditions of 1) no protruding vegetation (the control) and 2) with protruding vegetation. The spatial domain covered Colorado, Wyoming, and portions of the surrounding states; 81% of this area is nonforested. The surface net radiation, energy, and moisture fluxes displayed considerable differences when protruding vegetation was included. For shrubs, the net radiation, sensible, and latent fluxes changed by an average of 12.7, 6.9, and -22.7 W m^{-2}, respectively. For grass and crops, these fluxes changed by an average of 6.9, -0.8, and -7.9 W m^{-2}, respectively. Daily averaged flux changes were as much as 5 times these seasonal averages. As such, the new parameterization represents a major change in surface flux calculations over more simplistic and less physically realistic approaches.

1. Introduction

It has long been recognized that snow plays a key role in influencing climate system elements (e.g., Wagner 1973; Dewey 1977; Namias 1985; Walsh et al. 1985; Baker et al. 1992; Karl et al. 1993; Ellis and Leathers 1999; Bamzai and Shukla 1999), including atmospheric, hydrological, and ecosystem processes. Given snow's function in governing atmospheric and land surface processes, it is imperative that local, regional, and global models used to simulate weather, climate, hydrologic, and ecological interactions correctly describe snow's seasonal evolution and its associated water and energy fluxes.

A number of authors (e.g., Loth and Graf 1998b; Pomeroy et al. 1998; Slater et al. 2001; Strack et al. 2003; Liston 2004; Strack et al. 2007) recognized two dominant deficiencies in how regional and global atmospheric models represent the development of seasonal snow cover and interactions among snow, vegetation, and other components of Earth's climate system. First, subgrid snow distributions and their influence on surface energy and moisture fluxes are omitted. Second, conditions of vegetation protruding above the snow cover are ignored along with the effects of protruding vegetation on surface energy balances. Addressing these deficiencies is crucial for successful model representations of Earth's weather and climate system.

In an effort to address the first deficiency, the Subgrid SNOW Distribution (SSNOWD) parameterization (Liston 2004) was developed to explicitly include subgrid snow-depth and snow-cover variabilities in the representation

Corresponding author address: Dr. Glen E. Liston, Cooperative Institute for Research in the Atmosphere, Colorado State University, Fort Collins, CO 80523-1375.
E-mail: liston@cira.colostate.edu

DOI: 10.1175/2010JCLI4028.1

of model-simulated snow-covered areas. From atmospheric and hydrological perspectives, the subgrid snow-depth distribution is an important quantity to include within coarse-scale models. In natural systems, finescale heterogeneous snow distributions are largely responsible for the mosaic of snow-covered and snow-free areas that develop as snow melts, and the impacts of these fractional areas must be quantified in order to realistically simulate grid-averaged surface fluxes (Liston 1999).

The second key snow-related deficiency in climate system models concerns how surface energy budget calculations are performed when snow cover is too shallow or windblown to completely bury the vegetation. While this process is well recognized in forested areas, and appropriate methods have been implemented to account for it (e.g., Betts and Ball 1997), this phenomenon also occurs in vast tracts of grassland, shrubland, and cropland landscapes. In these short-vegetation landscapes, the effects of vegetation protruding above snow are commonly disregarded; yet, they can have important consequences for the simulation of surface energy and moisture fluxes (e.g., Strack et al. 2003, 2007; Mahrt and Vickers 2005a,b; Bewley et al. 2007, 2010).

As snow cover melts, albedo over an area decreases (Fig. 1; USACE 1956; O'Neill and Gray 1973). However, in environments with shallow or windblown snow covers, taller vegetation is rarely completely obscured (Fig. 2a). Further, as the snow cover melts, underlying vegetation protrudes above the remaining snow surface, exposing and accelerating the melting process in areas with the thinnest snow cover. This produces a snow-covered and snow-free mosaic that further decreases area-averaged surface albedo (Fig. 2b). For these conditions, the snow albedo (i.e., the albedo of the snow itself) is relatively large (0.6–0.8) and the snow-free (e.g., vegetation, rock, or soil) and protruding-vegetation albedos are relatively small (0.1–0.2); the combined albedo is approximately equal to the area-fraction weight of the snow and snow-free and/or protruding vegetation albedo (e.g., Liston 1995, 1999, 2004; Strack et al. 2007). The combined albedo decreases as the snow cover thins and shrinks in extent and the underlying surface is exposed and/or more vegetation protrudes above the snow surface.

Unfortunately, in most models the albedo decrease due to subgrid fractional snow cover and/or protruding vegetation is represented as a reduction in *snow* albedo instead of a reduction in *combined* albedo. This is not a sufficient representation of reality. Figure 3 displays the simple empirical functions used to define snow-depth versus snow-covered-fraction relationships used in 14 different land surface hydrology models and their associated general circulation models (GCMs), as well as

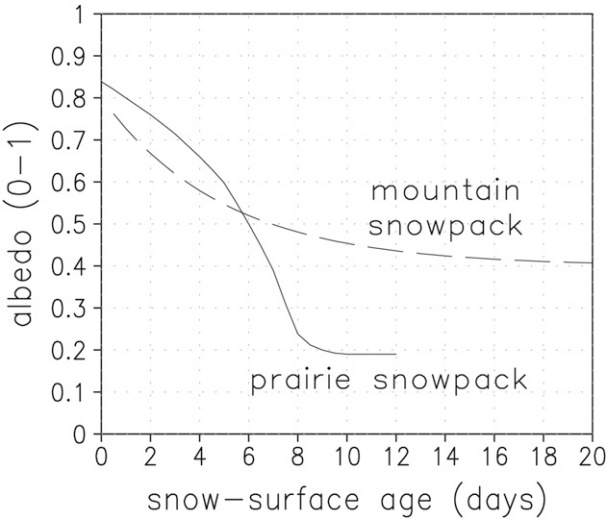

FIG. 1. Temporal albedo variation of a melting snow cover for the case of a deep (>1 m) mountain snowpack (U.S. Army Corps of Engineers 1956) and a shallow (<0.25 m) prairie snow cover (O'Neill and Gray 1973).

in one regional atmospheric model. With few exceptions, these models use the snow-covered fraction to weight the snow-covered and snow-free and/or protruding vegetation albedo values to obtain an averaged albedo. This averaged albedo is then used as part of a single surface energy balance calculation that assumes a completely snow-covered grid cell (but with a reduced albedo, as in Fig. 1). This approach is physically inappropriate: energy balances over snow-covered and snow-free areas are not identical, and the differences between them are nonlinear (Liston 1999, 2004). In contrast to the snow-free surface, the snow-covered energy balance requires a calculation that accounts for melting snow and the associated 0°C maximum snow-surface temperature constraint. The ultimate result of this albedo-averaging approach is that the modeled ''snow'' albedo becomes unrealistically low during ablation, and the snowmelt rates simulated by the model are faster than in the natural system (e.g., Liston 2004). In addition, related surface energy and moisture fluxes are grossly misrepresented (Liston 1999, 2004). Liston (2004) defined the role subgrid snow-depth variability has on defining the curves shown in Fig. 3. The parameterization described herein quantifies the contribution to these curves resulting from protruding vegetation.

Accounting for vegetation that protrudes above snow represents an opportunity to make valuable model improvements to snow evolution processes and land–atmosphere surface fluxes. Vegetation protruding through the snow has a direct and considerable impact on the surface energy balance and its temporal evolution (Fig. 2).

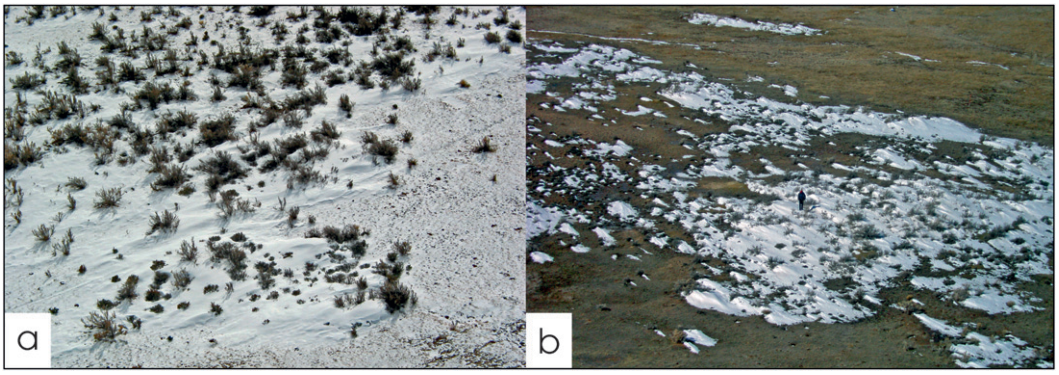

FIG. 2. Shrubs and grass protruding from (a) continuous and (b) discontinuous snow cover. For a scale reference, individual shrubs in (a) are 0.3–1.0 m in diameter and there is a person standing in the center of (b). These oblique photographs were taken from the top of a 32-m tower.

Within atmospheric modeling communities, quantifying plant–snow interactions has only recently received attention. Viterbo and Betts (1999) showed that putting the snow underneath the boreal forest canopy, instead of on top of the canopy, significantly reduced the European Centre for Medium-Range Weather Forecasts (ECMWF) modeled cold low-level temperature bias during spring. Strack et al. (2003) showed that including grass and shrubs protruding above the snow surface in a regional atmospheric model improved the simulation accuracy.

While minimal quantitative consideration has been directed to snow–vegetation interactions within grasslands and shrublands, recent studies show that during the snow season they play important roles in Earth's climate system (Pomeroy et al. 1997, 2003; Sturm et al. 2001, 2005a, b; Liston et al. 2002; Strack et al. 2003, 2007; Essery and Pomeroy 2004; Lee and Mahrt 2004; Mahrt and Vickers 2005a,b; Chapin et al. 2005; McCartney et al. 2006). Shrubland and grassland environments compose 68% of the seasonally snow-covered Northern Hemisphere (excluding Greenland) land surface (Liston 2004). These regions are snow covered for much of the winter and the vegetation is rarely completely obscured by snow (Fig. 2). While the importance of snow–vegetation interactions (Burke et al. 1989; Knight 1994) and ecosystem processes (Burke 1989; Gilmanov et al. 2004; Obrist et al. 2004) in these systems has been detailed, little quantitative work on grass– and shrub–snow–atmosphere interactions has been done (e.g., Lee and Mahrt 2004; Mahrt and Vickers 2005b).

Given the need to improve nonforested snow–vegetation interaction representations in Earth system models, we developed a field observation and modeling program to establish and describe the dominant features and processes associated with the seasonal evolution of snow in grassland and shrubland environments and their atmospheric interactions. Field observations were used to define key factors regarding vegetation height and distribution characteristics, as well as how snow accumulates within these landscapes. Observed snow–vegetation relationships were joined into a modeling framework that allowed analyses of how different land surface representations influence the resultant surface fluxes.

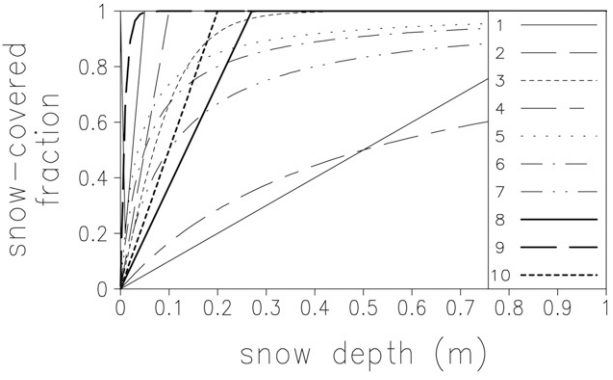

FIG. 3. Snow-fraction parameterizations used within 14 land surface and large-scale atmospheric models. Grid-averaged snow albedo is typically obtained by fractionally weighting the snow albedo and snow-free albedo according to these snow-covered fractions. The plotted curves correspond to the following land surface and atmospheric model names and references: 1) Land Surface Model/version 3 of the Community Climate Model (LSM/CCM3; Bonan 1996), ECHAM (Loth and Graf 1998a); 2) the Canadian Land Surface Scheme/(CLASS)/CCC > (Verseghy 1991), the Climate Version of the Regional Atmospheric Modeling System (ClimRAMS; Liston and Pielke 2001); 3) the Biosphere–Atmosphere Transfer Scheme (BATS; Yang et al. 1997); 4) BATS/CCM2,3 (Dickinson et al. 1993), the Community Land Model (CLM)/CCM3 (Zeng et al. 2002; Dai et al. 2003); 5) Action de Recherche Petite Echelle Grande Echelle (ARPEGE; Douville et al. 1995), ECHAM4 (Roesch et al. 1999); 6) CCM1 (Marshall and Oglesby 1994); 7) the original version of the CCM (CCM0A; Marshall et al. 1994); 8) the second Simple Biosphere Model/ Colorado State University model (SIB2/CSU; Sellers et al. 1996); 9) EM (Edelmann et al. 1995); and 10) BASE (Slater et al. 1998). See Liston (2004) for additional details.

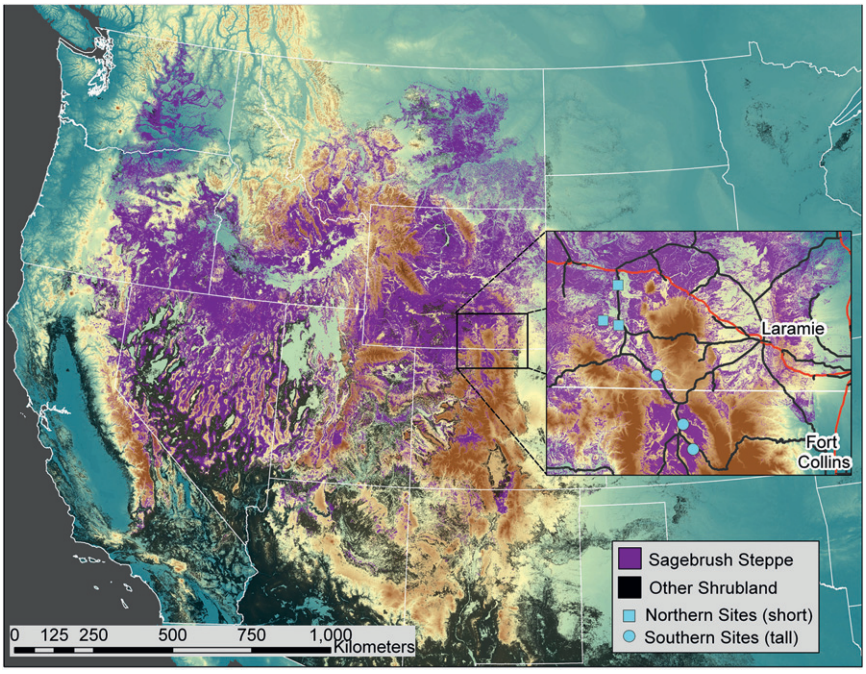

FIG. 4. National Gap Analysis Program (Maxwell et al. 2010) data from the central and western United States show the importance of sagebrush steppe (10%) and other shrublands (16%) in the contiguous United States. Grasslands, croplands, and forests (not highlighted) cover an additional 14%, 30%, and 21% of this domain, respectively; the remaining 9% includes bare, urban, riparian, and water areas. Our field site locations are highlighted in the inset figure; circles indicate high-elevation (deeper snow) sites while squares denote low-elevation sites.

Our objective is to describe a methodology for use in atmospheric, hydrological, and ecological modeling systems to account for first-order energy budget interactions among grasslands, shrublands, and croplands; snow; and the atmosphere. Further, we answer two essential questions. First, building on our field observations, how can we best represent (in the form of an earth system model subgrid parameterization) the surface energy budget influence of vegetation protruding through snow cover? Second, what is the impact of that protruding vegetation on local- to continental-scale surface energy and moisture fluxes?

2. Model description

a. Snow–vegetation observations

During the winters of 2004/05 through 2007/08, we conducted snow and vegetation surveys over six 1 km × 1 km sites located in north-central Colorado and south-central Wyoming (Fig. 4; C. A. Hiemstra et al. 2010, unpublished manuscript). During two winters (2005/06 and 2006/07), intensive biweekly measurements were conducted at all sites during the snow season (Fig. 5).

Snow measurement protocols included fine- and coarse-scale depth observations on the boundaries of two randomly located rectangular areas within each of the sites: a 50 m × 50 m area with depths measured every 25 cm along the boundary, and a 200 m × 800 m area with depth measurements approximately every 3–5 m along that boundary. The smaller finescale square was aligned with its axes parallel and perpendicular to the prevailing wind direction. The 25-cm horizontal spacing provided detailed information about the local snow–vegetation interactions. The larger coarse-scale domain provided a landscape survey of how snow depths and vegetation heights varied in response to area topographic and vegetation density variations. The larger area's long axis was aligned with the prevailing topographic slope. The more general distribution of the six main sites provided a measure of the regional snow and vegetation variations that can be expected in these short-vegetation environments.

Snow depths (assumed to be accurate to within ±1.5 cm) were measured along the rectangle boundaries using MagnaProbes (M. Sturm and J. Holmgren, 1999, self-recording snow depth probe, U.S. Patent 5,864,059), which are self-recording snow depth probes linked to a high-resolution (submeter horizontally) global positioning

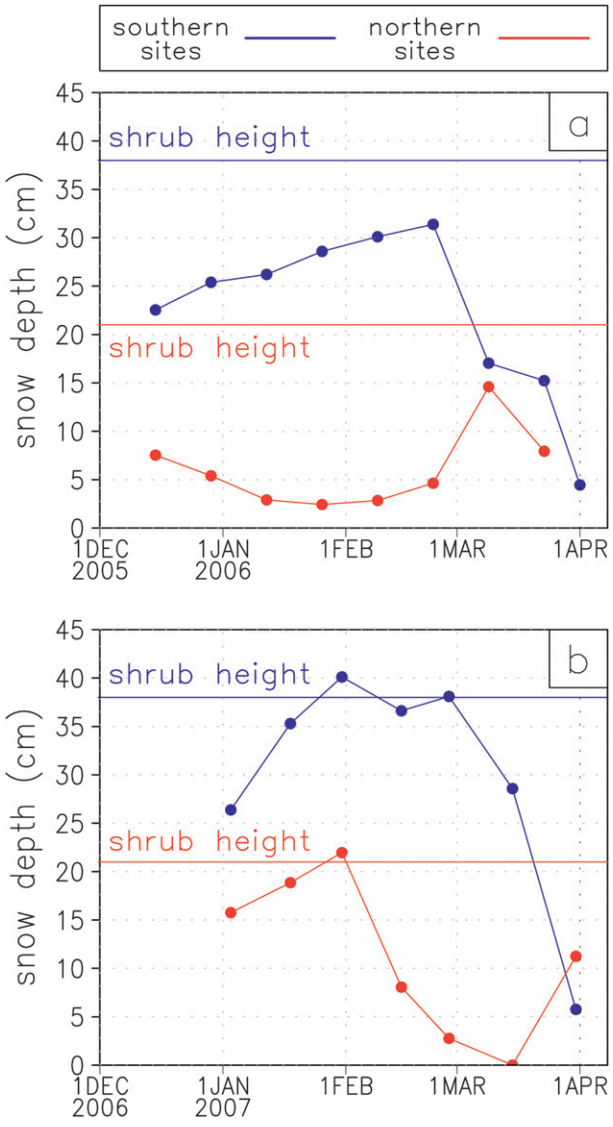

FIG. 5. Observed snow depth during each site visit (solid markers) for the 3 southern and 3 northern sites (Fig. 4) during (a) 2005/06 and (b) 2006/07. Also shown are the mean shrub heights for the southern and northern sites.

system (GPS) for the 3–5-m observations and which are linked to surveyed (horizontal accuracy of ±5 cm) points for the 25-cm observations. Snow densities were measured from two snow pit profiles located near the finescale depth measurements during each site visit. Project field observations produced 132 000 snow depth measurements. Of the four observation years, the winters of 2005/06 and 2006/07 had the shallowest and deepest snow accumulations, respectively. For that reason we chose those 2 yr for the model simulations presented herein.

All six sites are sagebrush steppe dominated by *Artemesia tridentata* shrubs (big sagebrush), which occupy over 36 million ha in the contiguous United States (Fig. 4; West and Young 2000; Welch 2005). The southernmost three sites are higher in elevation (2388–2563 m) and are dominated by *A. tridentata* ssp. *vaseyana* (mountain big sagebrush), which tends to be taller in stature (3–98 cm high, 38-cm mean height, $N = 1046$). In contrast, the northernmost three sites are lower in elevation (2093–2182 m) and are dominated by *A. tridentata* ssp. *wyomingensis* (Wyoming big sagebrush), which is shorter in stature (3–49 cm high, 21-cm mean height, $N = 1002$). The topographic variation among all sites was small, with elevation differences (maximum minus minimum) among the six sites ranging from 43 to 121 m.

Vegetation heights and winter snow accumulations in the three southern sites were greater than those in the three northern sites (Fig. 5). A conceptual feeling for what these numbers represent, and the overarching assumption guiding the snow–vegetation surface flux parameterization (e.g., the general case of vegetation protruding above the snow surface, instead of snow accumulating on and covering the vegetation), can be found in Fig. 2a, where the shrub heights are often higher than that of the snow. These general and detailed observations were used to guide the development of the following protruding vegetation parameterization.

b. Snow–grass–shrub parameterization

With respect to the atmosphere, vegetation protruding above the snow represents an absorber and reradiator of solar energy. Including this within the context of a surface energy budget (e.g., contained within an atmospheric, terrestrial model, and/or coupled climate system model) requires performing energy balance calculations over snow-covered and exposed vegetation portions of the domain. For reasons detailed in Liston (1995, 1999, 2004), we advocate performing two separate energy balances for each model grid cell, one over snow and one over vegetation, and fractionally weighting the resulting fluxes. Within each model grid cell and for each vegetation type, the areal fraction (when viewed from above) of the exposed vegetation in that grid cell F_v is the product of vegetation fraction Γ_v and the vegetation fraction protruding above snow γ_v:

$$F_v = \Gamma_v \gamma_v. \tag{1}$$

In addition, the snow-covered fraction is given by

$$F_s = 1 - \Gamma_v \gamma_v. \tag{2}$$

Defining the protruding vegetation fraction requires approximating the individual vegetation element's shape. For example, in the natural system, shrubs can be close

together and generally continuous, or they can be isolated bushes separated by bare ground or other vegetation such as grass. For the case of individual shrubs where the increase in exposed branch area, when viewed from above, increases linearly with decreasing snow depth, or for shrubs that are parabolic in shape, the variation of exposed branches with snow depth is given by

$$\gamma_v = \max\left[0, \left(1 - \frac{z_s}{z_v}\right)\right], \tag{3}$$

where z_s is the snow depth and z_v is the vegetation height. Under conditions where the individual shrubs are hemisphere shaped, the fraction of exposed branches is

$$\gamma_v = \max\left[0, \left(1 - \frac{z_s^2}{z_v^2}\right)\right]. \tag{4}$$

Our field observations do not indicate one of these shapes dominates over the other for western United States shrubs and grasses, but it is clear that sagebrush (*Artemisia tridentata* var. *vaseyana* and *Artemisia tridentata* var. *wyomingensis*) found in our research sites, and common canopy dominants throughout the western United States, generally grows as isolated plant elements separated by either grass and/or bare ground (Fig. 2; C. A. Hiemstra et al. 2010, unpublished manuscript).

The above equations can be generalized for the case where more than one vegetation type is present within a model grid cell:

$$F_v = \sum_{i=1}^{n} \Gamma_{v_i} \gamma_{v_i} \tag{5}$$

and

$$F_s = 1 - \sum_{i=1}^{n} \Gamma_{v_i} \gamma_{v_i}, \tag{6}$$

where i is the vegetation type, n is the number of vegetation types in the grid cell, and the other terms and associated equations are modified with the appropriate indices to handle multiple vegetation types.

To calculate grid-cell energy fluxes, two surface energy balance calculations are performed: one assuming the grid cell is snow covered and a second assuming the grid cell is snow free with the surface characteristics of protruding vegetation (assuming both calculations see the same atmosphere). Each surface energy balance component of these two calculations is then fractionally weighted in proportion to the snow-covered and protruding-vegetation fractions:

$$Q_{\text{ga}} = F_s Q_{\text{snow}} + F_v Q_{\text{veg}}, \tag{7}$$

where, for any flux variable Q, Q_{ga} is the grid-averaged flux; Q_{snow} is the snow-covered flux; and Q_{veg} is the protruding-vegetation flux.

c. *SnowModel*

To quantify the impacts of this snow–vegetation parameterization on surface energy balance calculations, we performed model simulations using SnowModel (Liston and Elder 2006a), a spatially distributed snow-evolution modeling system designed for application in all landscapes, climates, and conditions where snow occurs. It is an aggregation of four submodels: EnBal (Liston 1995; Liston et al. 1999), which calculates surface energy exchanges; SnowPack (Liston and Hall 1995), which simulates snow depth and water-equivalent evolution; SnowTran-3D (Liston and Sturm 1998; Liston et al. 2007), which accounts for snow redistribution by wind; and SnowAssim (Liston and Hiemstra 2008), which is available to assimilate field and remote sensing datasets.

SnowModel is designed to run on horizontal grid increments of 1–200 m and temporal increments of 10 min to 1 day. It can be applied using much larger grid increments (up to tens of kilometers) if the inherent loss in high-resolution (subgrid) information (Liston 2004) is acceptable. Processes simulated by SnowModel include the accumulation from snow precipitation; blowing-snow redistribution and sublimation; interception, unloading, and sublimation within forest canopies; snow-density evolution; and snowpack ripening and melt. SnowModel incorporates first-order physics required to simulate the snow evolution within each of the global snow classes [i.e., ice, tundra, cold taiga (or taiga), warm taiga (or alpine), prairie, maritime, and ephemeral], as defined by Sturm et al. (1995) and G. E. Liston and M. Sturm (2010, unpublished manuscript). An attractive feature of the distributed SnowModel snow-evolution modeling system is its realism in both physical processes and spatial and temporal distributions; it can drift snow at high elevations while simultaneously melting valley snow within the same domain.

For the simulations presented herein, the conductive flux at the soil–snow interface was assumed negligible and a near-surface soil temperature of −1°C was prescribed. In addition, the soil moisture fraction was set to 1.0 under the assumption that during snowmelt there is an abundance of moisture available. This approximation is further justified because during the model simulation period grass and shrubs are dormant and vegetation processes and fluxes associated with transpiration are minimal. Required SnowModel inputs include temporally

varying fields of precipitation, wind speed and direction, air temperature, and relative humidity, obtained from meteorological stations and/or an atmospheric model located within or near the simulation domain; and spatially distributed, time-invariant fields of topography and vegetation type.

d. MicroMet

Meteorological forcings required by SnowModel were provided by MicroMet (Liston and Elder 2006b), a quasi-physically based, high-resolution (e.g., 1-m to 10-km horizontal grid increment), meteorological distribution model. MicroMet is a data assimilation and interpolation model that utilizes meteorological station datasets and/or gridded atmospheric model or analyses datasets. MicroMet minimally requires screen-height air temperature, relative humidity, wind speed and direction, and precipitation data. The model uses known relationships between meteorological variables and the surrounding landscape (primarily topography) to distribute those variables over any given landscape in physically plausible and computationally efficient ways. MicroMet performs two kinds of adjustments to the meteorological data: 1) all available data, at a given time, are spatially interpolated over the domain and 2) physically based submodels are applied to each MicroMet variable to quantify the topographic, elevation, and vegetation effects at any given point in space and time. Station interpolations (horizontal) to a regular grid are done using a Barnes objective analysis scheme (Barnes 1964, 1973; Koch et al. 1983). The Barnes scheme applies a Gaussian distance-dependent weighting function, where the weight that a station contributes to the value of the grid point decreases with increasing distance from the observation. Interpolation weights are objectively determined as a function of data spacing and distribution. At each time step, MicroMet distributes the air temperature, relative humidity, wind speed, wind direction, incoming solar radiation, incoming longwave radiation, surface pressure, and precipitation, and makes them accessible to SnowModel.

MicroMet and SnowModel have been used to distribute observed and modeled meteorological variables, and evolve snow distributions over complex terrain in Colorado; Wyoming; Idaho; Oregon; Alaska; Arctic Canada; Siberia; Japan; Tibet; Chile; Germany; Austria; Svalbard, Norway; Greenland; and Antarctica as part of a wide variety of terrestrial modeling studies (e.g., Liston and Sturm 1998, 2002; Greene et al. 1999; Liston et al. 1999, 2000, 2002, 2007, 2008; Prasad et al. 2001; Hiemstra et al. 2002, 2006; Hasholt et al. 2003; Bruland et al. 2004; Liston and Winther 2005; Mernild et al. 2006, 2008, 2009; Liston and Hiemstra 2008).

3. Model simulations

a. Model configuration and simulation domain

Snow-evolution and surface energy fluxes were simulated from 1 October 2005 through 30 June 2006 and 1 October 2006 through 30 June 2007, spanning the driest and wettest winters of our 4-yr field observation program, respectively. Our simulations span the entire snow season, from the initial fall snow accumulation through complete spring ablation. Each simulation covered an 1180 km $\times$ 1000 km simulation domain centered on Colorado, Wyoming, and fractions of adjacent states (Fig. 6). This area is particularly conducive to studying grassland, shrubland, and cropland processes, since 81% of this domain is covered by these vegetation classes (forest, 17%; tall shrubs, 2%; short shrubs, 25%; grass, 40%; crops, 14%; and bare, 2%). Model simulations were performed using a 1-km horizontal grid increment (1 180 000 grid cells) and 1-h time step.

Vegetation data used in the model simulations were derived from the 30-m 2001 National Land Cover Data dataset (Homer et al. 2007) and the more-detailed sagebrush distributions provided by the western United States Sagebrush and Grassland Ecosystem Map Assessment Project (SAGEMAP; information online at http://sagemap.wr.usgs.gov/). The data were resampled (nearest neighbor) to 50 m and reclassified into corresponding SnowModel vegetation classes (Fig. 6; Liston and Elder 2006a). Vegetation heights required in the simulations were defined following existing field observations (C. A. Hiemstra et al. 2010, unpublished manuscript) to be (Fig. 6) forest, 10.0 m; tall shrub, 0.38 m; short shrub, 0.21 m; grass, 0.10 m; crops, 0.20 m; and bare, 0.01 m. Topography data were derived from the 30-m National Elevation Dataset (U.S. Geological Survey 2008). For the 1-km grid increment model simulations, the 50-m vegetation data were used to calculate vegetation-type fractions in each 1-km model grid cell, and the vegetation and topography data were resampled to create corresponding 1-km datasets (Fig. 6).

The topography and land cover of the study area are typical of the Great Plains (Sims and Risser 2000) and Rocky Mountain (Peet 2000) regions (Fig. 6). The weather is continental and dry with relatively high summer and low winter temperatures. The landforms shift from the eastern edge of the flat, rolling plains and tablelands to the dissected western canyons and high peaks of the Rocky Mountain Cordillera. As a reflection of the interaction between the atmosphere and land surface, the land cover changes from agricultural cropland, pastures, and grasslands in the east, to irrigated fields, conifer-dominated mountain forests, and vast tracts of sagebrush (the taller

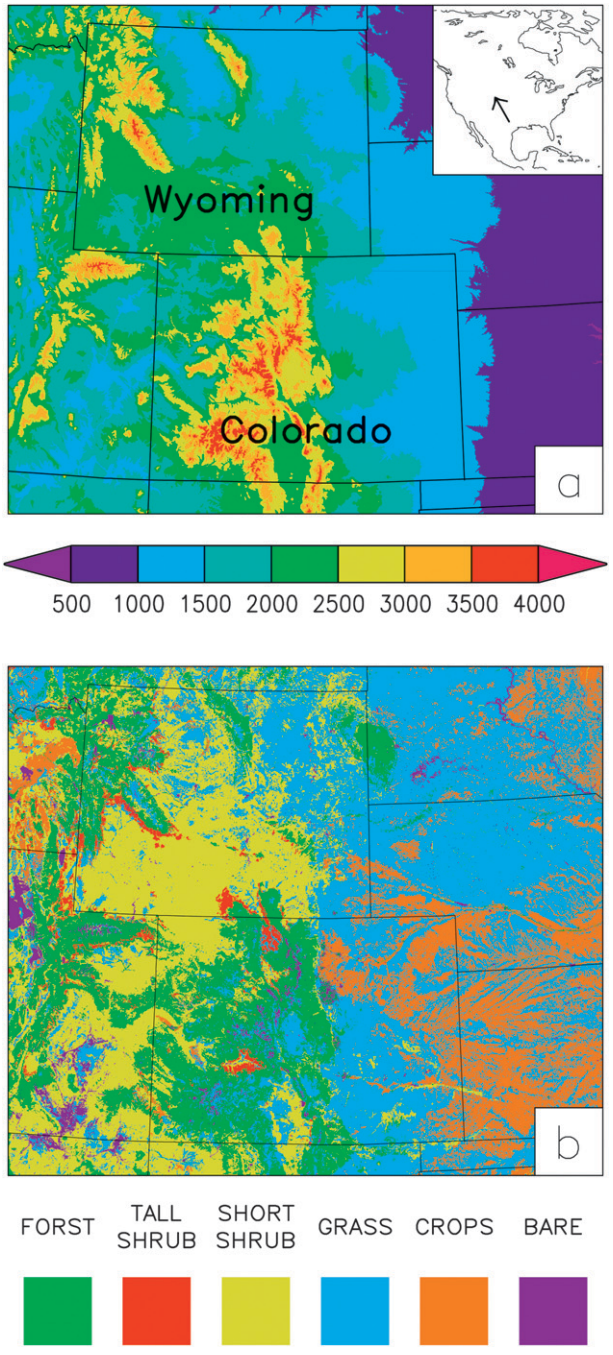

FIG. 6. Simulation domain (a) topography (m) and general location (arrow in inset), and (b) vegetation.

Artemisia tridentata var. *vaseyana* and shorter *Artemisia tridentata* var. *wyomingensis*) steppe in the west.

Winter weather over the simulation domain is dominated by frequent migratory high and low pressure systems associated with the polar jet stream and its associated polar front. If the jet stream flow is zonal, air masses associated with this front are Pacific in origin, producing substantial orographic snows in the mountains, and relatively mild air and minimal precipitation downwind (east) of these barriers. In the eastern Great Plains part of the domain, Arctic high pressure systems travel southward over the region, producing the area's coldest weather of the year. Upslope snow-precipitation events frequently occur in the western Great Plains during these cold outbreaks. Spring is a transition season when higher sun angles typically produce warmer days, yet cold air masses occasionally travel southward bringing heavy snows to the eastern part of the domain. In this area, March and April are often the snowiest months of the year.

b. *Meteorological forcing*

Meteorological data used in the model simulations were from two sources: the Local Analysis and Prediction System (LAPS) atmospheric analysis package (McGinley et al. 1991; Albers 1995; Albers et al. 1996; Birkenheuer 1999; Hiemstra et al. 2006), which provided air temperature, relative humidity, wind speed, and wind direction; and the North American Land Data Assimilation System (NLDAS; Mitchell et al. 2004), which contributed precipitation forcing.

LAPS was run by the National Oceanic and Atmospheric Administration's (NOAA) Earth System Research Laboratory (ESRL), using a 10-km horizontal grid (125 × 105) with 21 isobaric vertical levels and hourly temporal resolution. The LAPS analysis domain covers Colorado, Wyoming, and parts of the surrounding states. These analyses incorporated a wide range of observational datasets, including 1) surface observations from regional surface networks every 5 min to 3 h, 2) hourly surface aviation observations, 3) Doppler radar volume scans every 6–10 min, 4) wind and temperature Radio Acoustic Sounding System (RASS) profiles from the NOAA Demonstration Profiler Network every 6–60 min, 5) satellite visible data every 15–30 min, 6) multispectral image and sounding radiance data every 60 min, 7) GPS total precipitable water vapor determined from signal delay, and 8) automated aircraft observations. The resulting LAPS outputs include spatially and temporally continuous atmospheric state variables over the analysis domain (Liston et al. 2008).

To prepare the LAPS meteorological datasets for the model simulations, the MicroMet preprocessor (Liston and Elder 2006b) was used to process the original data. First, missing values were identified. Second, the preprocessor performed three quality assurance–quality control (QA–QC data) tests following Meek and Hatfield (1994): test 1 checked for values outside acceptable ranges, test 2 looked for consecutive values that exceed acceptable increments, and test 3 found constant consecutive

values with no observed change. Third, the preprocessor filled the missing data with calculated values; this was done in a variety of ways, all designed to preserve the diurnal cycles and other characteristics of the remaining data (see Liston and Elder 2006b for additional details).

The NLDAS precipitation data (Cosgrove et al. 2003) used in the simulations are a merging of Climate Prediction Center (CPC) daily continental United States (CONUS) gauge data with Parameter–Elevation Regressions on Independent Slopes Model (PRISM) topographical adjustments, CPC daily North American gauge data, hourly National Centers for Environmental Prediction (NCEP) stage II precipitation data (a national, 4-km, hourly analysis using hourly Doppler radar data), half-hourly CPC morphing technique (CMORPH) precipitation data, and 3-hourly North American Regional Reanalysis (NARR) precipitation data. This merging is designed to take advantage of the accuracy of the daily gauge product and the temporal and spatial resolutions of the Doppler radar and CMORPH products. The hourly NLDAS data are available on a $\frac{1}{8}^\circ$ grid covering the conterminous United States.

As part of the model simulations, MicroMet identified which meteorological variables were available from the collection of possible LAPS and NLDAS grid points, and used those to create the hourly, 1-km atmospheric forcing distributions required by SnowModel (air temperature, relative humidity, wind speed and direction, precipitation, and incoming solar and longwave radiation). The 1-km atmospheric fields were ingested by SnowModel to simulate the time evolution and spatial distribution of water and energy fluxes and states. Simulated variables included surface temperature, albedo, outgoing longwave radiation, latent heat flux, sensible heat flux, liquid precipitation, solid precipitation, snowmelt, sublimation, runoff, snow depth, snow density, and snow water equivalent.

4. Model results

For each of the simulation years (2005–06 and 2006–07), we performed full surface energy balance calculations for no protruding vegetation (the control) and with protruding vegetation. The protruding vegetation fraction was defined as the fraction of a unit ground area covered by vegetation when viewed from above. Radiation emitted or absorbed by the vegetation and snow was defined to be proportional to the vegetation fraction and the complement of the vegetation fraction, respectively. The simulations assumed shrubs had a parabolic shape [Eq. (3)] and calculated a protruding vegetation fraction that decreased linearly, from fully exposed to 0, as snow depth increased from 0 m to the vegetation canopy height.

Our objective was to isolate the contribution of protruding vegetation on surface energy and moisture fluxes [as opposed to quantifying the flux contribution resulting from subgrid snow-depth distributions modifying the snow-covered fraction in the absence of vegetation, e.g., Liston (2004)]. Therefore, the control simulations assumed complete snow cover in a given grid cell when the snow depth in that grid cell was greater than zero. For the protruding vegetation simulations, individual shrubs and other vegetation elements were assumed to be parabolic in shape, and the vegetation fraction in each grid cell was assumed to be 1.0 (i.e., one land cover type per grid cell). Thus, our modeling system used MicroMet–SnowModel to perform the snow-depth evolution and surface energy balance calculations, and the resulting fluxes were fractionally weighed using Eq. (7) with the snow-covered and protruding-vegetation weights defined by Eqs. (1)–(3).

The 2005/06 and 2006/07 snow seasons were different, with more snow falling (Fig. 7) and lasting longer (Fig. 8) in 2006/07 than in 2005/06. While snow residence time was similar between years in the western half of the domain's mountains and basins, the eastern half had roughly twice as many snow days in 2006/07 as in 2005/06. This is consistent with our coincident field observations (C. A. Hiemstra et al. 2010, unpublished manuscript).

The fraction of each vegetation class containing snow evolved over time and varied among years (Fig. 9). The fraction was calculated by dividing all snow-covered grid cells of a particular class type by the number of total cells for each class type for each day of the simulation. Since grass and crops possess similar residence-time characteristics and they dominate the eastern half of the simulation domain (Fig. 8), grass and crops were aggregated (Fig. 9). The ephemeral nature of winter snow cover in the eastern part of the domain was particularly pronounced in 2005/06. The tall shrub vegetation class is typically located at higher elevations and exhibited longer snow-covered winters.

As snow falls in these nonforested vegetation environments (and also in the forests), canopy-intercepted snow exposed to wind is quickly dislodged from the twigs and branches and accumulates on the ground below. Conceptually, we could think of these short-vegetation elements as trees, where the winter's accumulated snow-precipitation depth is comparable to the tree height. The fraction of vegetation protruding above the snow, for each vegetation class during the simulations, is displayed in Fig. 10. These protruding vegetation elements (e.g., stems, twigs, branches, seeds, and winter leaves), with their relatively low albedos and ability to heat to temperatures

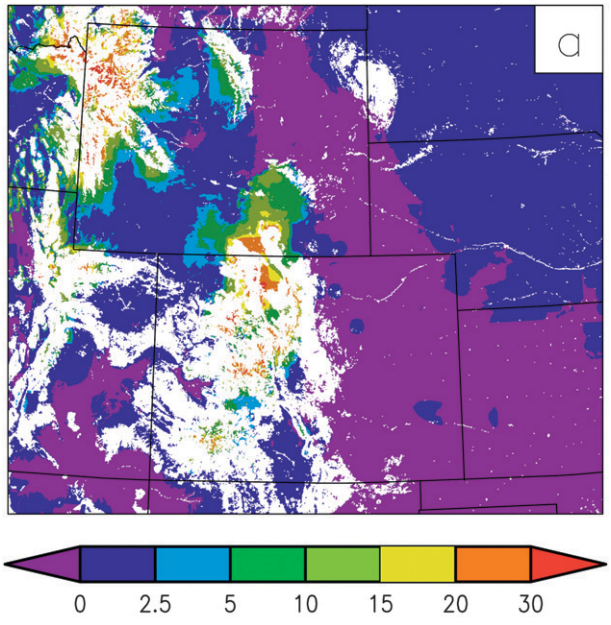

FIG. 7. Snow-water-equivalent depth (cm) on 1 Jan (a) 2006 and (b) 2007. Forested areas are masked out (white).

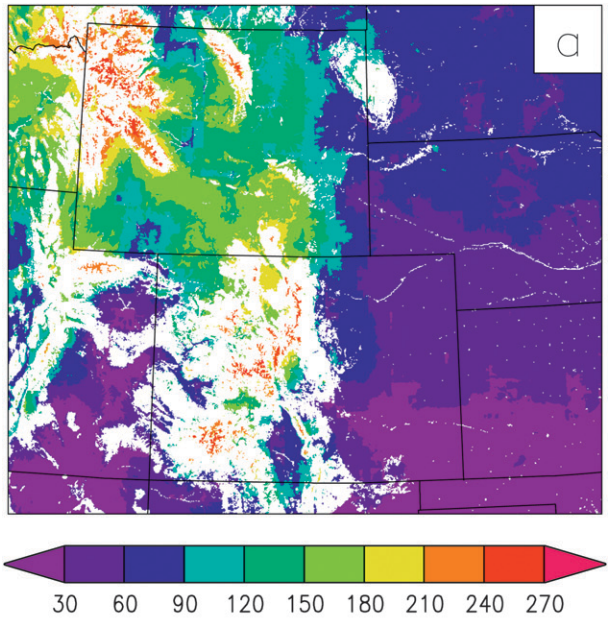

FIG. 8. Number of days with snow during (a) 2005/06 and (b) 2006/07. Forested areas are masked out (white).

above freezing, are efficient collectors of solar radiation, radiate longwave radiation, and modify local sensible and latent fluxes (e.g., Mahrt and Vickers 2005b). On average, for all vegetation classes and both simulation years, a significant fraction of the vegetation within each vegetation class was protruding above the snow (Fig. 10). Only the tall shrubs, which generally exist at higher elevations with relatively deep snowpacks, come close to being snow covered for much of the snow season.

The effects of protruding vegetation on the spatial distribution of surface energy budget components are shown in Figs. 11 (2005/06) and 12 (2006/07). The net radiation for all vegetation types was increased by including vegetation elements in the calculations (Figs. 11c and 12c), with the smallest changes occurring in the tall shrubs and high-elevation vegetation that remained snow covered during much of the snow season. The biggest changes occurred in the short shrub, grass, and crop

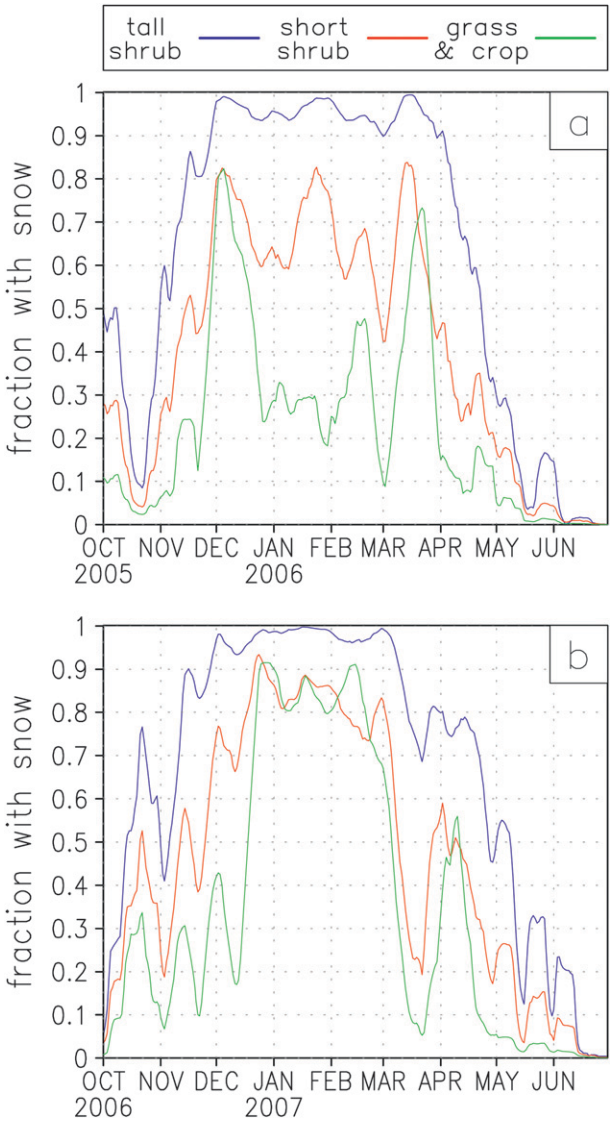

FIG. 9. Fraction of each vegetation class that contained snow, for tall shrubs, short shrubs, and combined grass and crops, during (a) 2005/06 and (b) 2006/07. A 10-day line smoother was applied to damp out the episodic nature of the snow distributions and improve readability.

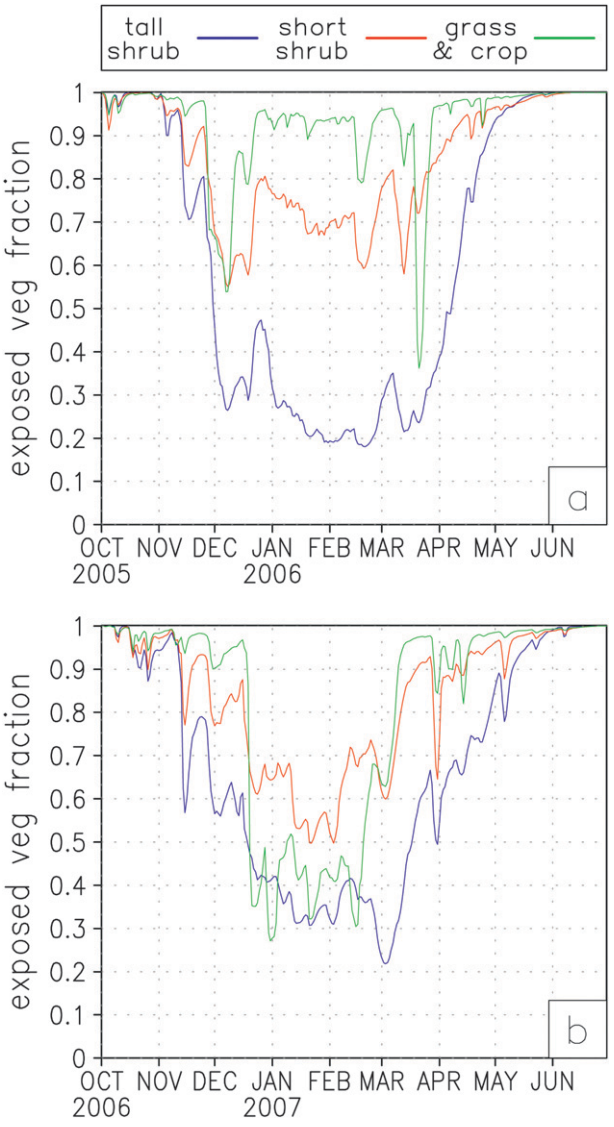

FIG. 10. Fraction of vegetation height protruding above the snow, averaged over the vegetation classes of tall shrubs, short shrubs, and combined grass and crops, during (a) 2005/06 and (b) 2006/07.

regions where snow precipitation depths are similar in magnitude to the vegetation heights. This is true for the 2005/06 and 2006/07 simulations. Sensible and latent heat fluxes showed the greatest change in short shrub areas of the simulation domain when protruding vegetation was included. Short shrubs frequently have a greater percentage of their branches protruding above the snow (because the depth of the accumulated snow precipitation is frequently comparable to, or less than, the shrub heights). Increased heating at the surface (Figs. 11f and 12f), and increased (more negative) moisture transport away from the surface (Figs. 11i and 12i), were evident throughout shrub, grassland, and cropland areas.

To illustrate the impacts of representing grass and shrubs protruding through snow, the average daily net radiation, sensible, and latent fluxes were averaged for each vegetation class throughout the simulations. The resulting temporal patterns were similar for tall and short shrubs, and for grass and crops; therefore, we present aggregated averages for these two groups (Figs. 13 and 14, Table 1).

Including protruding shrubs in our simulations increased the domain-averaged surface net radiation by

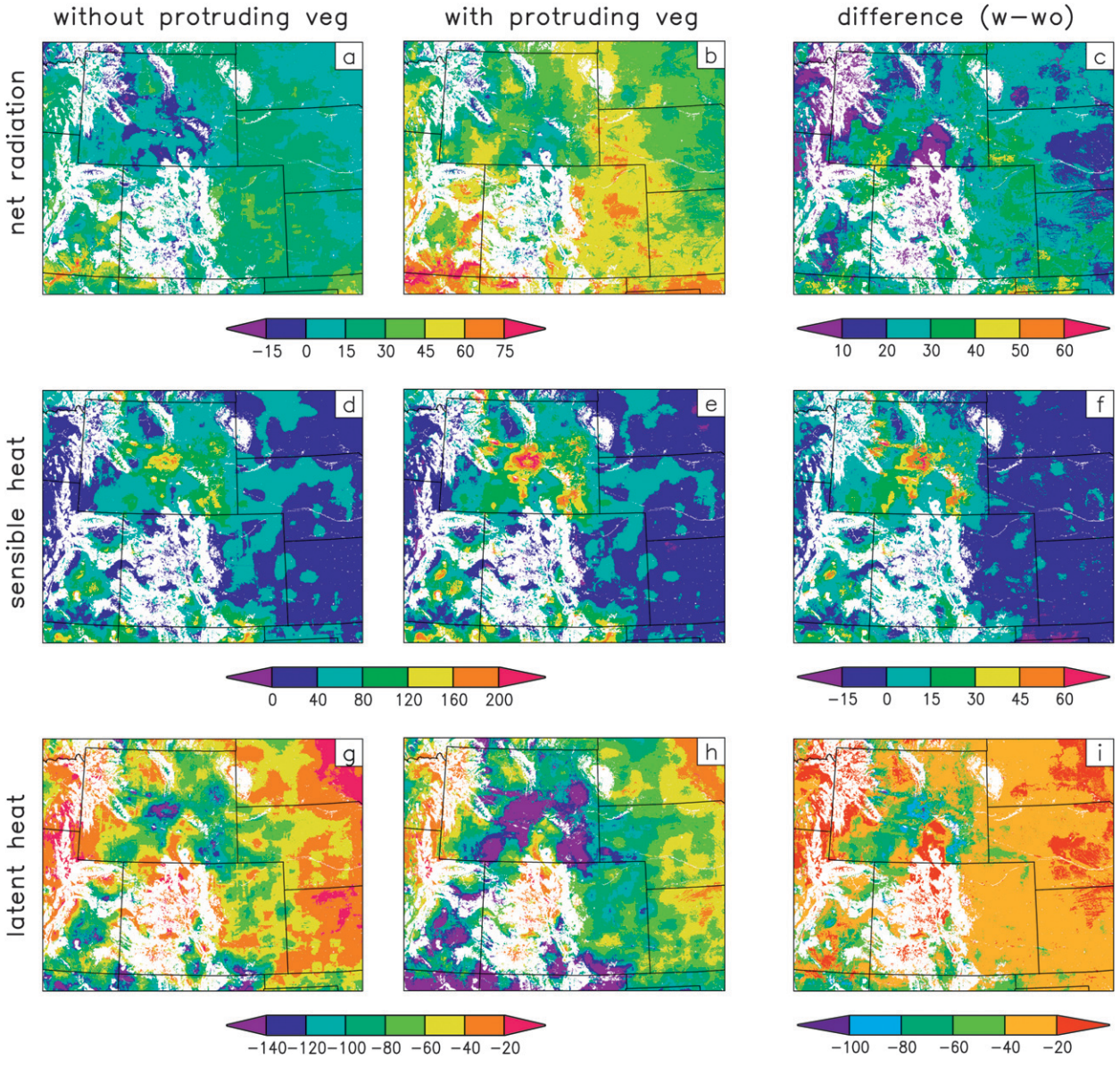

FIG. 11. The 2005/06 snow-season-averaged surface fluxes (W m^{-2}); positive fluxes are toward the surface. Shown are the net radiation for (a) the control (vegetation covered by snow), (b) with protruding vegetation, and (c) the difference [(b) − (a)]; the sensible heat flux for (d) the control (vegetation covered by snow), (e) with protruding vegetation, and (f) the difference [(e) − (d)]; and the latent heat flux for (g) the control (vegetation covered by snow), (h) with protruding vegetation, and (i) the difference [(h) − (g)]. Forested areas are masked out (white).

9.7 W m^{-2}, sensible heat flux by 5.9 W m^{-2}, and latent heat flux (more negative) by −18.5 W m^{-2} in 2005/06 (the residual of these numbers represents a change in snowmelt energy). In 2006/07, the domain-averaged surface net radiation increased by 15.7 W m^{-2}, the sensible heat flux by 7.9 W m^{-2}, and the latent heat flux (more negative) by −26.8 W m^{-2} (Table 1). The magnitude of these changes is greater for the shrub case than the grass/crop case (Table 1); these differences occur because the shorter grass and crop vegetation types generally have a smaller fraction of protruding vegetation above the snow surface.

5. Discussion

This study focused on snow–vegetation–atmosphere interactions that are not typically included within current earth system models used within scientific and

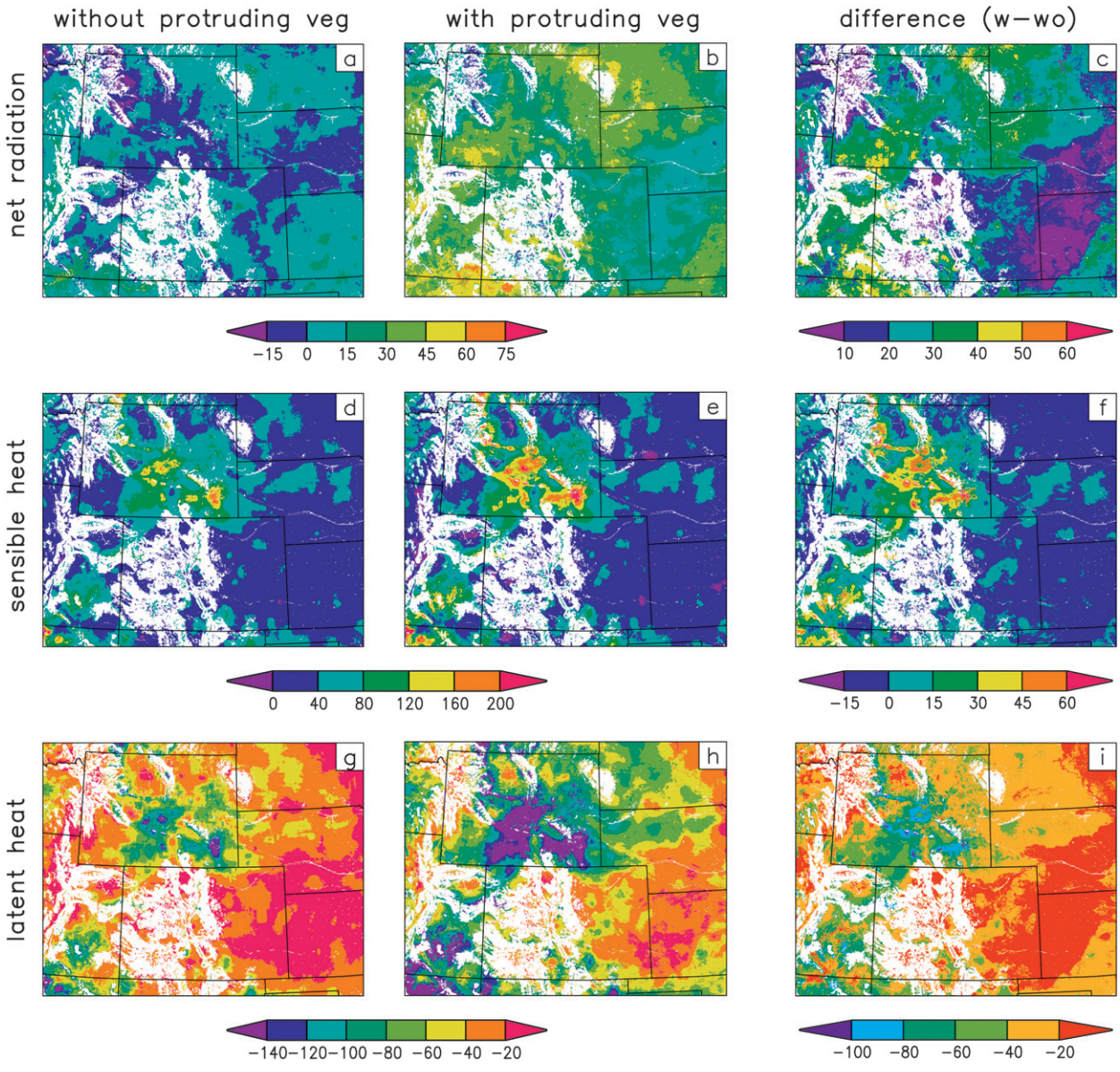

FIG. 12. As in Fig. 11, but for 2006/07.

resource-management communities. In particular, it highlights the importance of accounting for nonforest vegetation (e.g., grass and shrubs) protruding above snow-covered surfaces in the modeled surface energy balances. Surface net radiation, energy, and moisture fluxes displayed considerable differences when the protruding vegetation parameterization was applied; this was true for tall and short shrubs, and grass and crops (Table 1). In general, protruding vegetation absorbs more incoming solar radiation than the snow surface. This increases the surface net radiation and sensible heat flux, decreases (more negative) the latent heat flux, and the balance modifies the melt flux. For shrubs, the net radiation, sensible, and latent fluxes changed by an average of 12.7, 6.9, and -22.7 W m^{-2}, respectively, over the two simulated snow seasons when protruding shrubs were accounted for. For grass and crops, these same fluxes changed by an average of 6.9, -0.8, and -7.9 W m^{-2}, respectively, over the simulation periods. Maximum daily averaged changes for all fluxes reached as high as 5 times these seasonally averaged values (Figs. 13 and 14, Table 1). As such, this parameterization represents a major change in the surface flux calculations over more simplistic and less realistic approaches. Instead of defining the grid-averaged albedo to be the combination of the snow and protruding vegetation fractions and calculating a single

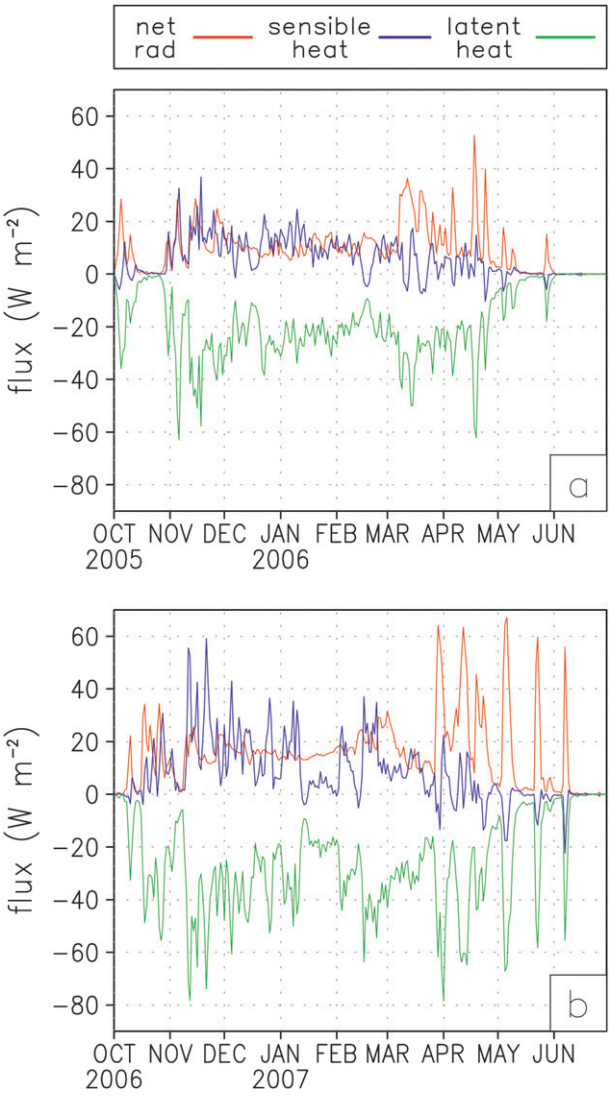

FIG. 13. Energy flux differences (with protruding vegetation − control) averaged over tall and short shrub classes, for net radiation, sensible heat flux, and latent heat flux. Positive fluxes are toward the surface during (a) 2005/06 and (b) 2006/07.

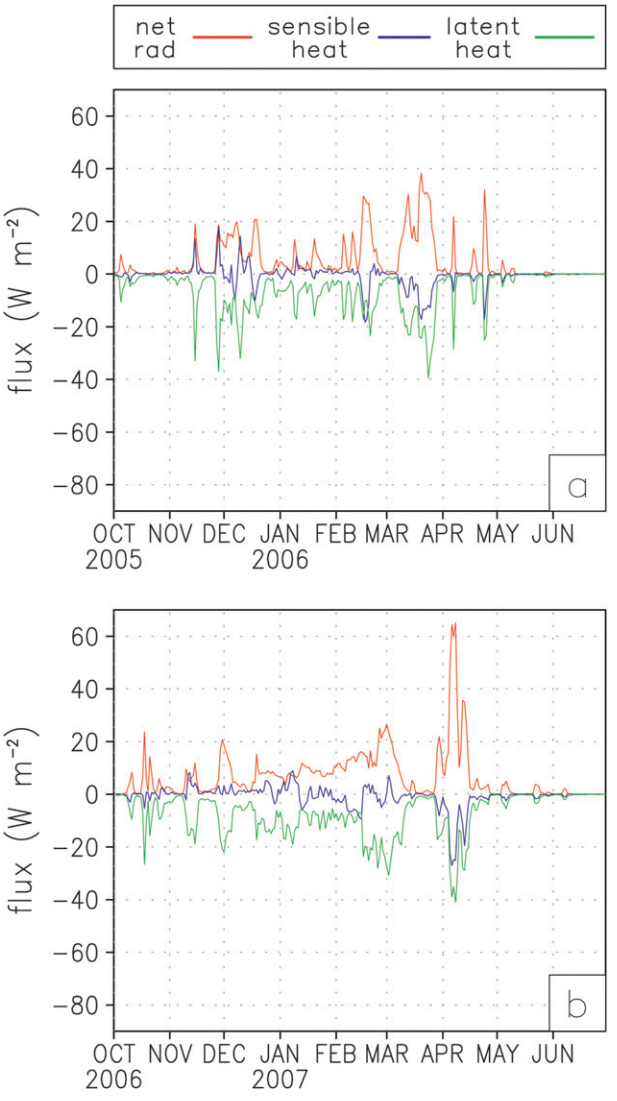

FIG. 14. As in Fig. 13, but averaged over grass and crop classes.

energy budget, this parameterization advocates using separate energy balances for the snow-covered and protruding vegetation fractions of each model grid cell, and fractionally weighting these fluxes to define grid-average quantities that are returned to the overlying atmospheric model.

In addition to suggesting that separate energy balances be performed for snow-covered and protruding vegetation fractions of each model grid cell, this study intimates that the snow-fraction parameterizations presented in Fig. 3 actually represent the combined influence of protruding vegetation and subgrid snow-depth variability. With this understanding, improvements to these curves are easily achievable. For example, the assumption of uniform snow depth and parabolic-shaped shrubs covering the entire grid cell leads to the linear parameterizations in Fig. 3, where the snow depth corresponding to a snow-covered fraction of 1.0 equals the vegetation height. Therefore, the application of vegetation height datasets allows the linear parameterizations in Fig. 3 to vary spatially over a model's simulation domain. Similarly, global distributions of vegetation heights, in combination with subgrid snow distribution information (e.g., Liston 2004) and some assumptions about the relationships between the two, can be used to more realistically define all of the Fig. 3 curves.

Defining the amount of vegetation protruding above the snow cover requires predefining vegetation characteristics such as canopy heights, the fraction of each grid

TABLE 1. Statistics of the energy flux differences (with protruding vegetation − control) presented in Figs. 13 and 14 for tall and short shrub classes, and grass and crop classes (W m^{-2}). Positive fluxes are toward the surface. The residuals of the averages represent a change in snowmelt energy.

	2005/06			2006/07		
	Avg	Min	Max	Avg	Min	Max
Tall and short shrubs						
Net radiation	9.7	0.0	52.7	15.7	0.0	67.2
Sensible flux	5.9	−10.4	36.9	7.9	−22.3	59.1
Latent flux	−18.5	−62.9	0.0	−26.8	−78.4	0.0
Grass and crops						
Net radiation	6.0	0.0	38.3	7.7	0.1	65.0
Sensible flux	−0.7	−18.3	18.1	−0.9	−27.1	8.9
Latent flux	−7.1	−39.4	0.0	−8.6	−41.0	−0.1

cell covered by each short vegetation type, and some estimate of the vertical configuration of each vegetation element (e.g., parabolic or hemispheric). The vegetation fraction can be determined from higher-resolution vegetation datasets. Defining vegetation heights over large areas is still in its infancy, although substantial progress has been made by combining various remote sensing datasets with field observations (e.g., Kellndorfer et al. 2004; Mundt et al. 2006; Homer et al. 2009).

In addition to vegetation characteristics, the time evolution of spatial snow-depth distributions must be known. It is typical for earth system models to evolve the snow-water-equivalent depth as part of their simulations, and models exist (e.g., Verseghy 1991; Essery et al. 1999; Liston et al. 2007) that evolve snow density as a function of time, temperature, wind transport, and snowfall history; they can also convert water equivalent to snow depth.

The simulations described herein were performed with a land surface model that was uncoupled from the atmosphere (SnowModel was driven with prescribed atmospheric forcing instead of having a modeled atmosphere that evolved as part of the surface energy flux calculations). Because of the lack of two-way interactions in the simulations, the results represent a reallocation of the surface energy budget terms and quantities in the simulations; the incoming solar and longwave radiation were the same in both simulations. Additional simulations using regional or global coupled land–atmosphere models would likely lead to further insights into climate system feedbacks associated with the new parameterization and the roles of exposed vegetation with respect to snow season climate, including the direct feedback to near-surface air temperature and the associated changes in snowmelt fluxes.

In this application we did not consider the effects of subgrid snow-depth distributions; here, we have only considered the horizontal and vertical vegetation distributions relative to a uniform snow depth and single vegetation type with 100% fractional coverage over each grid cell. Our field observations suggest this is an oversimplification of the natural system (C. A. Hiemstra et al. 2010, unpublished manuscript); in reality, we observed spatial variations in vegetation height and spacing over distances corresponding to individual shrubs (submeter). In addition, our field observations show that snow depth also varies spatially. Such subgrid snow-depth distributions also play a role in defining the amount of protruding vegetation and defining the fractional snow-covered area. Including subgrid spatial snow depth variations would add an additional level of complexity to the parameterization and improve the physical realism of the natural system. In addition, our consideration of vegetation shape (e.g., parabolic or hemispheric) has not included a method to account for solar radiation striking the side of the individual vegetation elements; it assumes the vertically projected area or footprint is available to absorb radiation and modify the surface energy balance. This yields a conservative estimate of the influence of protruding shrubs on the surface energy budget.

Sturm et al. (2005a) introduced the ratio (λ) of snow depth (z_s) to vegetation height (z_v) that defines conditions where protruding vegetation has important energy balance consequences:

$$\lambda(t) = \frac{z_s(t)}{f(t)\, z_v}, \tag{8}$$

where t is time and f is a vegetation compression factor that ranges from 0.1 (high compression) to 1.0 (low compression) depending on how much the vegetation is bent over and reduced in height by the snow. At the Sturm et al. (2005a) high-latitude observation site, and for some shrub species, f was substantially less than 1.0. For the dominant western United States shrub species in our study, *Artemisia tridentata*, we found $f \approx 1.0$. Our grassland observations indicate that grass leaves and stems bend over depending on grass species, height, density, and snow conditions (i.e., $f < 1.0$). In grasslands there is a seasonal variation as well. Leaves that were upright and resilient in fall become prostrate by midwinter due to leaf and stem comminution through high winds, decomposition, and previous snow accumulation. Sturm et al. (2005a) noted that, in addition to branch and stem strength and suppleness, f can also depend on precipitation conditions. For example, if the air temperature is near freezing during a snow precipitation event, snow is more likely to adhere to the branches and accumulate to the bending point.

From the perspective of the snow-season surface energy budget, Eq. (8) suggests two important regimes.

When the snow depth is much greater than the vegetation height ($\lambda > 1$) for much of the season, the surface energy budget will be dominated by the snow surface and protruding vegetation is not very important. When the snow depth is comparable to, or less than, the vegetation height ($\lambda \leq 1$), budget calculations require consideration of snow and protruding vegetation. Field observations suggest throughout much of the snow-covered nonforested world that mid- to late-winter snowpack depths are comparable to the vegetation height. While this may be coincidental (and we do not think it is, for the reasons listed below), this has been found to be generally true in 1) high-latitude grassland and tundra areas (Benson and Sturm 1993; Liston and Sturm 1998, 2002; Essery et al. 1999; Sturm et al. 2001; Sturm and Liston 2003); 2) midlatitude prairie, shrubland, grassland, and crop regions such as those found in central Canada and the central and western United States (Pomeroy et al. 1993; Pomeroy and Gray 1995; C. A. Hiemstra et al. 2010, unpublished manuscript); 3) high-latitude mountainous areas like the Brooks Range in Arctic Alaska, and Svalbard, Norway (Winther et al. 1998; Bruland et al. 2004; Liston and Sturm 2002; Essery et al. 2005); and 4) midlatitude treeless mountaintops such as those found in Idaho, Utah, and western Colorado and Wyoming (Elder et al. 1991, 1995, 1998; Greene et al. 1999; Balk and Elder 2000; Prasad et al. 2001; Hiemstra et al. 2002, 2006).

These nonforested regions combine to cover the majority of Earth's seasonally snow-covered land surface (Liston 2004). All of these areas share low winter temperatures (which suppress precipitation amounts) and minimal orographic lifting (which would generally produce larger precipitation values). Importantly, a key reason why these regions frequently have snowpack depths comparable to the vegetation height is that many of these short-vegetation regions repeatedly experience wind speeds sufficient to transport snow (Sturm et al. 1995; Liston 2004; G. E. Liston and M. Sturm 2010, unpublished manuscript). This does two things: it redistributes the general snow cover into deeper topographic drift traps, such as the lee of ridges and river cut-banks, and it produces blowing-snow sublimation. Depending on the blowing-snow suspended transport, and the atmospheric conditions of the air temperature, humidity, wind speed, and incoming solar radiation, blowing-snow sublimation can return between 5% and 50% of the winter snow precipitation to the atmosphere (e.g., Liston and Sturm 2004), causing an important reduction in snow. Because of the snow-trapping ability of the vegetation, and the reduced wind speeds within vegetation canopies, blowing-snow sublimation generally occurs when the snow depth is greater than the vegetation height (e.g., Liston and Sturm 1998; Sturm et al. 2001; Liston et al. 2002); blowing-snow sublimation shuts down when the snowpack is reduced back to the vegetation height and the snow within the vegetation canopy is unable to be moved by most naturally occurring winds. Thus, there are environmental mechanisms that constrain snow depths to be similar to nonforested vegetation heights.

6. Conclusions

Earth system models are known to oversimplify many aspects of their coupling between land and atmosphere. Detailed representations of snow-related processes have been particularly lacking, including ways to account for the impacts of vegetation protruding above the snow surface on modeled surface energy and moisture fluxes. To help correct this deficiency, we developed a subgrid parameterization for use within regional and global atmospheric, hydrologic, and ecologic modeling systems to account for the first-order, energy budget interactions between grasslands and shrublands, snow, and the atmosphere.

The nonforested landscapes where this parameterization applies represent 68% of the seasonally snow-covered Northern Hemisphere land surface (excluding Greenland). In addition, these areas contain snow for significant portions of the year, ranging from days and weeks to several months. As such, it is important to appropriately represent surface energy fluxes over these surfaces. One of the reasons why these snow–vegetation–atmosphere interactions are important is because protruding vegetation is so prevalent in these winter landscapes; this occurs because the time-integrated winter solid precipitation (i.e., the snow accumulation) is frequently of similar or lower magnitude than the height of these relatively short vegetation types. Conceptually, during winter, these vegetation types interact with the atmosphere in a similar way to forests, which also typically extend above the snow surface.

The parameterization requires knowing how much vegetation is protruding above the snow cover. This requires two vegetation-related data layers in the land surface model: one describing the vegetation height or, at a minimum, a table that associates each model vegetation type with a corresponding vegetation height and a second layer that defines the shrub or grassland vegetation fraction in each grid cell. In addition, the snow depth (as opposed to the more hydrologically significant water-equivalent depth) at each grid cell and each time step must be known. This combined information, along with an assumption of the shape (e.g., parabolic or hemispherical), allows for the calculation of the areal

fraction of the grid cell that has vegetation protruding above the snow surface.

Knowledge of the protruding vegetation fraction, and the associated improvement in surface flux calculations, has the potential to provide important improvements to earth system model simulations of fall, winter, and spring land–atmosphere interactions. In addition, the locations where these snow and vegetation processes are important and cover large areas, ranging in scale from local to regional and continental. As a consequence, these kinds of improvements to the simulation of land surface processes allow us to advance our ability to appropriately simulate climate system processes, interactions, feedbacks, and evolution.

Acknowledgments. The authors thank Dan Birkenheuer for kindly providing the LAPS datasets. This work was supported by NASA Grants NNG04GP59G and NNX08AI03G.

REFERENCES

Albers, S. C., 1995: The LAPS wind analysis. *Wea. Forecasting,* **10,** 342–352.

——, J. A. McGinley, D. L. Birkenheuer, and J. R. Smart, 1996: The Local Analysis and Prediction System (LAPS): Analyses of clouds, precipitation, and temperature. *Wea. Forecasting,* **11,** 273–287.

Baker, D. G., D. L. Ruschy, R. H. Skaggs, and D. B. Wall, 1992: Air temperature and radiation depressions associated with a snow cover. *J. Appl. Meteor.,* **31,** 247–254.

Balk, B., and K. Elder, 2000: Combining binary decision tree and geostatistical methods to estimate snow distribution in a mountain watershed. *Water Resour. Res.,* **36,** 13–26.

Bamzai, A. S., and J. Shukla, 1999: Relation between Eurasian snow cover, snow depth, and the Indian summer monsoon: An observational study. *J. Climate,* **12,** 3117–3132.

Barnes, S. L., 1964: A technique for maximizing details in numerical weather map analysis. *J. Appl. Meteor.,* **3,** 396–409.

——, 1973: Mesoscale objective analysis using weighted time-series observations. NOAA Tech. Memo. ERL NSSL-62, 60 pp. [NTIS COM-73-10781.]

Benson, C. S., and M. Sturm, 1993: Structure and wind transport of seasonal snow on the Arctic slope of Alaska. *Ann. Glaciol.,* **18,** 261–267.

Betts, A. K., and J. H. Ball, 1997: Albedo over the boreal forest. *J. Geophys. Res.,* **102** (D24), 28 901–28 909.

Bewley, D., J. W. Pomeroy, and R. L. H. Essery, 2007: Solar radiation transfer through a subarctic shrub canopy. *Arct. Antarct. Alp. Res.,* **39,** 365–374.

——, R. L. H. Essery, J. W. Pomeroy, and C. Ménard, 2010: Measurements and modelling of snowmelt and turbulent heat fluxes over shrub tundra. *Hydrol. Earth Syst. Sci. Discuss.,* **7,** 1005–1032.

Birkenheuer, D., 1999: The effect of using digital satellite imagery in the LAPS moisture analysis. *Wea. Forecasting,* **14,** 782–788.

Bonan, G. B., 1996: A land surface model (LSM version 1.0) for ecological, hydrological, and atmospheric studies: Technical description and user's guide. NCAR Tech. Note NCAR/TN-417+STR, Boulder, CO, 150 pp.

Bruland, O., G. E. Liston, J. Vonk, and A. Killingtveit, 2004: Modelling the snow distribution at two high-Arctic sites at Svalbard, Norway, and at a sub-Arctic site in central Norway. *Nord. Hydrol.,* **35,** 191–208.

Burke, I. C., 1989: Control of nitrogen mineralization in a sagebrush steppe landscape. *Ecology,* **70,** 1115–1126.

——, W. A. Reiners, and R. K. Olson, 1989: Topographic control of vegetation in a mountain big sagebrush steppe. *Vegetatio,* **84,** 77–86.

Chapin, F. S., III, and Coauthors, 2005: Role of land-surface changes in arctic summer warming. *Science,* **310,** 657–660.

Cosgrove, B. A., and Coauthors, 2003: Real-time and retrospective forcing in the North American Land Data Assimilation System (NLDAS) project. *J. Geophys. Res.,* **108,** 8842, doi:10.1029/2002JD003118.

Dai, Y., and Coauthors, 2003: The Common Land Model. *Bull. Amer. Meteor. Soc.,* **84,** 1013–1023.

Dewey, K. F., 1977: Daily maximum and minimum temperature forecasts and the influence of snow cover. *Mon. Wea. Rev.,* **105,** 1594–1597.

Dickinson, R. E., A. Henderson-Sellers, and P. J. Kennedy, 1993: Biosphere Atmosphere Transfer Scheme (BATS) Version 1e as coupled to the NCAR Community Climate Model. NCAR Tech. Note NCAR/TN-387+STR, 72 pp.

Douville, H., J.-F. Royer, and J.-F. Mahfouf, 1995: A new snow parameterization for the Météo-France climate model. Part I: Validation in stand-alone experiments. *Climate Dyn.,* **12,** 21–35.

Edelmann, W., D. Majewski, E. Heise, P. Prohl, G. Doms, B. Ritter, M. Gertz, and T. Hanisch, 1995: *Dokumentation des EM/DMSystems*. Deutscher Wetterdienst, 550 pp. [Available from Deutscher Wetterdienst, Zentralamt, D-63004 Offenbach am Main, Germany.]

Elder, K., J. Dozier, and J. Michaelsen, 1991: Snow accumulation and distribution in an alpine watershed. *Water Resour. Res.,* **27,** 1541–1552.

——, J. Michaelsen, and J. Dozier, 1995: Small basin modeling of snow water equivalence using binary regression tree methods. *Biogeochemistry of Seasonally Snow-Covered Catchments,* K. Tonnessen, M. Williams, and M. Tranter, Eds., IAHS Publ. 228, 129–139.

——, W. Rosenthal, and R. E. Davis, 1998: Estimating the spatial distribution of snow water equivalence in a montagne watershed. *Hydrol. Processes,* **12,** 1973–1808.

Ellis, A. W., and D. J. Leathers, 1999: Analysis of cold airmass temperature modification across the U.S. Great Plains as a consequence of snow depth and albedo. *J. Appl. Meteor.,* **38,** 696–711.

Essery, R., and J. W. Pomeroy, 2004: Vegetation and topographic control of windblown snow distributions in distributed and aggregated simulations for an Arctic tundra basin. *J. Hydrometeor.,* **5,** 734–744.

——, E. Martin, H. Douville, A. Fernández, and E. Brun, 1999: A comparison of four snow models using observations from an alpine site. *Climate Dyn.,* **15,** 583–593.

——, E. Blyth, R. Harding, and C. Lloyd, 2005: Modelling albedo and distributed snowmelt across a low hill on Svalbard. *Nord. Hydrol.,* **36,** 207–218.

Gilmanov, T. G., D. A. Johnson, N. Z. Saliendra, T. J. Svejcar, R. F. Angell, and K. L. Clawson, 2004: Winter CO_2 fluxes above sagebrush-steppe ecosystems in Idaho and Oregon. *Agric. For. Meteor.,* **126,** 73–88.

Greene, E. M., G. E. Liston, and R. A. Pielke Sr., 1999: Simulation of above treeline snowdrift formation using a numerical snow-transport model. *Cold Reg. Sci. Technol.,* **30,** 135–144.

Hasholt, B., G. E. Liston, and N. T. Knudsen, 2003: Snow distribution modelling in the Ammassalik region, south east Greenland. *Nord. Hydrol.,* **34,** 1–16.

Hiemstra, C. A., G. E. Liston, and W. A. Reiners, 2002: Snow redistribution by wind and interactions with vegetation at upper treeline in the Medicine Bow Mountains, Wyoming, USA. *Arct. Antarct. Alp. Res.,* **34,** 262–273.

——, ——, and ——, 2006: Observing, modelling, and validating snow redistribution by wind in a Wyoming upper treeline landscape. *Ecol. Modell.,* **197,** 35–51.

Homer, C., and Coauthors, 2007: Completion of the 2001 National Land Cover Database for the conterminous United States. *Photogramm. Eng. Remote Sens.,* **73,** 337–341.

——, C. L. Aldridge, D. K. Meyer, M. J. Coan, and Z. H. Bowen, 2009: Multiscale sagebrush rangeland habitat modeling in southwest Wyoming. U.S. Geological Survey Open-File Rep. 2008-1027, 14 pp.

Karl, T. R., P. Y. Groisman, R. W. Knight, and R. R. Heim, 1993: Recent variations of snow cover and snowfall in North America and their relation to precipitation and temperature variations. *J. Climate,* **6,** 1327–1344.

Kellndorfer, J., W. Walker, L. Pierce, C. Dobson, J. A. Fites, C. Hunsaker, J. Vona, and M. Clutter, 2004: Vegetation height estimation from shuttle radar topography mission and national elevation datasets. *Remote Sens. Environ.,* **93,** 339–358.

Knight, D. H., 1994: *Mountains and Plains: The Ecology of Wyoming Landscapes*. Yale University Press, 338 pp.

Koch, S. E., M. DesJardins, and P. J. Kocin, 1983: An interactive Barnes objective map analysis scheme for use with satellite and conventional data. *J. Climate Appl. Meteor.,* **22,** 1487–1503.

Lee, Y.-H., and L. Mahrt, 2004: An evaluation of snowmelt and sublimation over short vegetation in land surface modeling. *Hydrol. Processes,* **18,** 3543–3557.

Liston, G. E., 1995: Local advection of momentum, heat, and moisture during the melt of patchy snow covers. *J. Appl. Meteor.,* **34,** 1705–1715.

——, 1999: Interrelationships among snow distribution, snowmelt, and snow cover depletion: Implications for atmospheric, hydrologic, and ecologic modeling. *J. Appl. Meteor.,* **38,** 1474–1487.

——, 2004: Representing subgrid snow cover heterogeneities in regional and global models. *J. Climate,* **17,** 1381–1397.

——, and D. K. Hall, 1995: An energy balance model of lake ice evolution. *J. Glaciol.,* **41,** 373–382.

——, and M. Sturm, 1998: A snow-transport model for complex terrain. *J. Glaciol.,* **44,** 498–516.

——, and R. A. Pielke Sr., 2001: A climate version of the Regional Atmospheric Modeling System. *Theor. Appl. Climatol.,* **68,** 155–173.

——, and M. Sturm, 2002: Winter precipitation patterns in Arctic Alaska determined from a blowing-snow model and snow-depth observations. *J. Hydrometeor.,* **3,** 646–659.

——, and ——, 2004: The role of winter sublimation in the Arctic moisture budget. *Nord. Hydrol.,* **35,** 325–334.

——, and J.-G. Winther, 2005: Antarctic surface and subsurface snow and ice melt fluxes. *J. Climate,* **18,** 1469–1481.

——, and K. Elder, 2006a: A distributed snow-evolution modeling system (SnowModel). *J. Hydrometeor.,* **7,** 1259–1276.

——, and ——, 2006b: A micrometeorological distribution system for high-resolution terrestrial modeling applications (MicroMet). *J. Hydrometeor.,* **7,** 217–234.

——, and C. A. Hiemstra, 2008: A simple data assimilation system for complex snow distributions (SnowAssim). *J. Hydrometeor.,* **9,** 989–1004.

——, J.-G. Winther, O. Bruland, H. Elvehøy, and K. Sand, 1999: Below-surface ice melt on the coastal Antarctic ice sheet. *J. Glaciol.,* **45,** 273–285.

——, ——, ——, ——, ——, and L. Karlöf, 2000: Snow and blue-ice distribution patterns on the coastal Antarctic ice sheet. *Antarct. Sci.,* **12,** 69–79.

——, J. P. McFadden, M. Sturm, and R. A. Pielke Sr., 2002: Modeled changes in Arctic tundra snow, energy, and moisture fluxes due to increased shrubs. *Global Change Biol.,* **8,** 17–32.

——, R. B. Haehnel, M. Sturm, C. A. Hiemstra, S. Berezovskaya, and R. D. Tabler, 2007: Simulating complex snow distributions in windy environments using SnowTran-3D. *J. Glaciol.,* **53,** 241–256.

——, C. A. Hiemstra, K. Elder, and D. W. Cline, 2008: Mesocell Study Area (MSA) snow distributions for the Cold Land Processes Experiment (CLPX). *J. Hydrometeor.,* **9,** 957–976.

Loth, B., and H.-F. Graf, 1998a: Modeling the snow cover in climate studies 1. Long-term integrations under different climatic conditions using a multilayered snow-cover model. *J. Geophys. Res.,* **103** (D10), 11 313–11 327.

——, and ——, 1998b: Modeling the snow cover in climate studies 2. The sensitivity to internal snow parameters and interface processes. *J. Geophys. Res.,* **103** (D10), 11 329–11 340.

Mahrt, L., and D. Vickers, 2005a: Boundary-layer adjustment over small-scale changes of surface heat flux. *Bound.-Layer Meteor.,* **116,** 313–330.

——, and ——, 2005b: Moisture fluxes over snow with and without protruding vegetation. *Quart. J. Roy. Meteor. Soc.,* **131,** 1251–1270.

Marshall, S., and R. J. Oglesby, 1994: An improved snow hydrology for GCMs. Part 1: Snow cover fraction, albedo, grain size, and age. *Climate Dyn.,* **10,** 21–37.

——, J. O. Roads, and G. Glatzmaier, 1994: Snow hydrology in a general circulation model. *J. Climate,* **7,** 1251–1269.

Maxwell, J., K. Gergely, J. Aycrigg, L. Duarte, and A. Davidson Eds., 2010: *Gap Analysis Bulletin.* No. 17, USGS/BRD/Gap Analysis Program, Moscow, ID, 48 pp.

McCartney, S. E., S. K. Carey, and J. W. Pomeroy, 2006: Spatial variability of snowmelt hydrology and its controls on the streamflow hydrograph in a subarctic catchment. *Hydrol. Processes,* **20,** 1001–1016.

McGinley, J. A., S. C. Albers, and P. A. Stamus, 1991: Validation of a composite convective index as defined by a real-time local analysis system. *Wea. Forecasting,* **6,** 337–356.

Meek, D. W., and J. L. Hatfield, 1994: Data quality checking for single station meteorological variables. *Agric. For. Meteor.,* **69,** 85–109.

Mernild, S. H., G. E. Liston, B. Hasholt, and N. T. Knudsen, 2006: Snow-distribution and melt modeling for Mittivakkat Glacier, Ammassalik Island, southeast Greenland. *J. Hydrometeor.,* **7,** 808–824.

——, ——, C. A. Hiemstra, and K. Steffen, 2008: Surface melt area and water balance modeling on the Greenland Ice Sheet 1995–2005. *J. Hydrometeor.,* **9,** 1191–1211.

——, ——, ——, and ——, 2009: Record 2007 Greenland Ice Sheet surface melt extent and runoff. *Eos, Trans. Amer. Geophys. Union,* **90,** 13–14.

Mitchell, K. E., and Coauthors, 2004: The multi-institution North American Land Data Assimilation System (NLDAS): Utilizing multiple GCIP products and partners in a continental distributed hydrological modeling system. *J. Geophys. Res.,* **109,** D07S90, doi:10.1029/2003JD003823.

Mundt, J. T., D. R. Streutker, and N. F. Glenn, 2006: Mapping sagebrush distribution using fusion of hyperspectral and lidar classifications. *Photogramm. Eng. Remote Sens.,* **72,** 47–54.

Namias, J., 1985: Some empirical evidence for the influence of snow cover on temperature and precipitation. *Mon. Wea. Rev.,* **113,** 1542–1553.

Obrist, D., D. Yakir, and J. A. Arnone, 2004: Temporal and spatial patterns of soil water following wildfire-induced changes in plant communities in the Great Basin in Nevada, USA. *Plant Soil,* **262,** 1–12.

O'Neill, A. D. J., and D. M. Gray, 1973: Spatial and temporal variations of the albedo of prairie snowpack. *Proc. Symp. on the Role of Snow and Ice in Hydrology,* Vol. 1, Banff, AB, Canada, UNESCO–WMO–IAHS, 176–186.

Peet, R. K., 2000: Forests and meadows of the Rocky Mountains. *North American Terrestrial Vegetation,* 2nd ed., M. G. Barbour, and W. D. Billings, Eds., Cambridge University Press, 75–121.

Pomeroy, J. W., and D. M. Gray, 1995: Snowcover accumulation, relocation and management. National Hydrology Research Institute Science Rep. 7. NHRI, Environment Canada, Saskatoon, SK, Canada, 144 pp.

——, ——, and P. G. Landine, 1993: The Prairie Blowing Snow Model: Characteristics, validation, operation. *J. Hydrol.,* **144,** 165–192.

——, P. Marsh, and D. M. Gray, 1997: Application of a distributed blowing snow model to the Arctic. *Hydrol. Processes,* **11,** 1451–1464.

——, D. M. Gray, K. R. Shook, B. Toth, R. L. H. Essery, A. Pietroniro, and N. Hedstrom, 1998: An evaluation of snow accumulation and ablation processes for land surface modeling. *Hydrol. Processes,* **12,** 2339–2367.

——, B. Toth, R. J. Granger, N. R. Hedstrom, and R. L. H. Essery, 2003: Variation in surface energetics during snowmelt in complex terrain. *J. Hydrometeor.,* **4,** 702–716.

Prasad, R., D. G. Tarboton, G. E. Liston, C. H. Luce, and M. S. Seyfried, 2001: Testing a blowing snow model against distributed snow measurements at Upper Sheep Creek, Idaho, USA. *Water Resour. Res.,* **37,** 1341–1357.

Roesch, A., H. Gilgen, M. Wild, and A. Ohmura, 1999: Assessment of GCM-simulated snow albedo using direct observations. *Climate Dyn.,* **15,** 405–418.

Sellers, P. J., and Coauthors, 1996: A revised land surface parameterization (SiB2) for atmospheric GCMs. Part I: Model formulation. *J. Climate,* **9,** 676–705.

Sims, P. L., and P. G. Risser, 2000: Grasslands. *North American Terrestrial Vegetation,* 2nd ed., M. G. Barbour and W. D. Billings, Eds., Cambridge University Press, 323–356.

Slater, A. G., A. J. Pitman, and C. E. Desborough, 1998: The validation of a snow parameterization designed for use in general circulation models. *Int. J. Climatol.,* **18,** 595–617.

——, and Coauthors, 2001: The representation of snow in land surface schemes: Results from PILPS 2(d). *J. Hydrometeor.,* **2,** 7–25.

Strack, J. E., R. A. Pielke Sr., and J. Adegoke, 2003: Sensitivity of model-generated daytime surface heat fluxes over snow to land-cover changes. *J. Hydrometeor.,* **4,** 24–42.

——, ——, and G. E. Liston, 2007: Arctic tundra shrub invasion and soot deposition: Consequences for spring snowmelt and near-surface air temperatures. *J. Geophys. Res.,* **112,** G04S44, doi:10.1029/2006JG000297.

Sturm, M., and G. E. Liston, 2003: The snow cover on lakes of the Arctic Coastal Plain of Alaska, U.S.A. *J. Glaciol.,* **49,** 370–380.

——, J. Holmgren, and G. E. Liston, 1995: A seasonal snow cover classification system for local to global applications. *J. Climate,* **8,** 1261–1283.

——, J. P. McFadden, G. E. Liston, F. S. Chapin III, C. H. Racine, and J. Holmgren, 2001: Snow–shrub interactions in Arctic tundra: A hypothesis with climatic implications. *J. Climate,* **14,** 336–344.

——, T. Douglas, C. Racine, and G. E. Liston, 2005a: Changing snow and shrub conditions affect albedo with global implications. *J. Geophys. Res.,* **110,** G01004, doi:10.1029/2005JG000013.

——, J. Schimel, G. Michelson, J. Welker, S. F. Oberbauer, G. E. Liston, J. Fahnestock, and V. E. Romanovsky, 2005b: Winter biological processes could help convert Arctic tundra to shrubland. *Bioscience,* **55,** 17–26.

U.S. Army Corps of Engineers, 1956: Snow hydrology. Summary Rep. of the Snow Investigations, USACE, 433 pp.

U.S. Geological Survey, cited 2008: National Elevation Dataset. EROS Data Center, Sioux Falls, SD. [Available online at http://ned.usgs.gov/.]

Verseghy, D. L., 1991: CLASS—A Canadian Land Surface Scheme for GCMs. I: Soil model. *Int. J. Climatol.,* **11,** 111–133.

Viterbo, P., and A. K. Betts, 1999: Impact on ECMWF forecasts of change to the albedo of the boreal forests in the presence of snow. *J. Geophys. Res.,* **104,** 27 803–27 810.

Wagner, A. J., 1973: The influence of average snow depth on monthly mean temperature anomaly. *Mon. Wea. Rev.,* **101,** 624–626.

Walsh, J. E., W. H. Jasperson, and B. Ross, 1985: Influences of snow cover and soil moisture on monthly air temperature. *Mon. Wea. Rev.,* **113,** 756–768.

Welch, B. L., 2005: Big sagebrush: A sea fragmented into lakes, ponds, and puddles. General Tech. Rep. RMRS-GTR-144, Rocky Mountain Research Station, U.S. Forest Service, Fort Collins, CO, 210 pp.

West, N. E., and J. A. Young, 2000: Intermountain valleys and lower mountain slopes. *North American Terrestrial Vegetation,* 2nd ed., M. G. Barbour and W. D. Billings, Eds., Cambridge University Press, 255–284.

Winther, J.-G., O. Bruland, K. Sand, A. Killingtveit, and D. Marechal, 1998: Snow accumulation distribution on Spitsbergen, Svalbard, in 1997. *Polar Res.,* **17,** 155–164.

Yang, Z.-L., R. E. Dickinson, A. Robock, and K. Y. Vinnikov, 1997: Validation of the snow submodel of the Biosphere–Atmosphere Transfer Scheme with Russian snow cover and meteorological observational data. *J. Climate,* **10,** 353–373.

Zeng, X., M. Shaikh, Y. Dai, R. E. Dickinson, and R. Myneni, 2002: Coupling of the Common Land Model to the NCAR Community Climate Model. *J. Climate,* **14,** 1832–1854.